Nonpolar $1T$-to-$1T'$ order-disorder transition in a MoS₂ monolayer

Xue Ma [1], Ningbo Fan,[1] Jinzhu Zhao [2,3,4] and Bin Xu [1,*]

[1]*Institute of Theoretical and Applied Physics, Jiangsu Key Laboratory of Thin Films, School of Physical Science and Technology, Soochow University, Suzhou 215006, China*

[2]*Guangdong Basic Research Center of Excellence for Structure and Fundamental Interactions of Matter, Guangdong Provincial Key Laboratory of Quantum Engineering and Quantum Materials, School of Physics, South China Normal University, Guangzhou 510006, China*

[3]*Guangdong-Hong Kong Joint Laboratory of Quantum Matter, Frontier Research Institute for Physics, South China Normal University, Guangzhou 510006, China*

[4]*Center for Computational Science and Engineering, Southern University of Science and Technology, Shenzhen 518055, China*

Finding two-dimensional (2D) materials with ferroelectricity is of great interests towards polarization-related applications and nanosized devices. Despite much theoretical efforts that predict the existence of novel 2D ferroelectrics, only a small portion have been realized in experiments. The well-known 2D transition-metal dichalcogenide molybdenum disulfide (MoS₂) monolayer was predicted to have a ferroelectric $d1T$ polymorph resulting from condensation of soft phonons from the centrosymmetric $1T$ phase. However, experiments mostly obtain a nonpolar monoclinic $1T'$ phase, whereas the $d1T$ phase has not been observed. In this study, we use various first-principles techniques, including density-functional theory total-energy calculations, *ab initio* molecular dynamics, and the temperature-dependent effective potential method to show that the nonpolar $1T'$ phase is thermodynamically more stable than the $d1T$ phase. Furthermore, the $1T$ phase at high temperature is averaged among degenerate $1T'$ structures, and the $1T$-to-$1T'$ transition upon cooling is predicted to be of first order with a strong order-disorder character. Effect of strain on the stable structure and the likely ground state of other MoX₂ (X = Se, Te) monolayers are also discussed.

DOI: [10.1103/PhysRevB.108.184101](https://doi.org/10.1103/PhysRevB.108.184101)

I. INTRODUCTION

The ever-growing interests in two-dimensional (2D) materials are intimately related to their crystal structures, which can significantly affect the mechanical, electronic, optical, and catalytic properties [1–6]. Among the large family of layered systems, a few with ferroelectricity form a special class, especially those exhibiting out-of-plane polarization, which hold great promise to be utilized in miniaturized functional devices. Interestingly, the most-studied 2D transition-metal dichalcogenide (TMD) MoS₂ is predicted to have a ferroelectric $d1T$ polymorph in its monolayer form [7].

Monolayer MoS₂ is known to crystallize in one of the two types of structures, differed by S-Mo-S intralayer stacking, viz., the 2H phase with Mo atom surrounded by six S atoms in trigonal prismatic coordination [8], and the $1T$ phase with the octahedrally coordinated Mo atom [9]. Although the 2H phase is thermodynamically more stable, the metastable $1T$ phase can be synthesized [10–12] and is of interests due to its superior electrical conductivity that can be used as electrodes to significantly improve the efficiency of electrochemical energy storage devices [13], as the structure of the $1T$ phase has larger interlayer spacing, allows faster charge transfer, and it is electrochemically more active than the 2H polymorph.

However, the centrosymmetric $1T$ phase is not stable at low temperature, since density-functional theory (DFT) calculations show that this structure has soft phonons, with the strongest at the reciprocal space points K (1/3,1/3,0) and M (1/2,0,0) [7,14]. Three low-energy structures that can be regarded as a distorted $1T$ phase have been studied previously, viz., the $d1T$, $1T'$, and $1T''$ phases. The $d1T$ phase is found theoretically to be associated with the K-point instability, such that Fermi nesting at $q \approx$ K point leads to a $\sqrt{3} \times \sqrt{3}$ supercell reconstruction. This structure has space group $P31m$, and it was predicted to be ferroelectric due to cooperative coupling between an out-of-plane polar mode with the in-plane trimerization mode [7]. Nevertheless, the effect of temperature was not considered in previous works, and $d1T$-MoS₂ has not been observed in experiments.

The $1T'$ phase can be regarded as being derived from the M-point soft mode, which has comparable imaginary frequency as that of the K point. It has a 2×1 superstructure relative to the $1T$ phase, by forming Mo dimer chains with distorted MoS₆ octahedra. The $1T'$ phase has almost the same energy as that of the $d1T$ phase according to DFT calculations [15], while interestingly it has been directly observed in experiments by scanning transmission electron microscopy [16–18] and is also consistent with the 2×1 unit cell found by scanning tunneling microscopy [19], indicating the possibility that the $1T'$ phase is thermodynamically more stable than $d1T$.

*binxu19@suda.edu.cn

The $1T''$ phase has a 2×2 supercell reconstruction from $1T$, with trimerization from three Mo atoms around one S atom in the unit cell. Trimerized Mo atoms squeeze half of the S atoms out of plane, giving rise to a weak polarization of about 0.04 $\mu C/cm^2$ [20], much smaller than that of the $d1T$ phase [7]. The total energy of the $1T''$ phase was predicted to be higher than that of the $d1T$ or $1T'$ phase [17], but it was, however, recently observed in experiment and was demonstrated to be ferroelectric at room temperature [20].

Therefore, it remains elusive (i) why the most occurring $1T$-like polymorph is the $1T'$ phase at room temperature, (ii) whether the ferroelectric $d1T$ phase can be stabilized at some intermediate temperature, and (iii) if the $1T''$ phase can be a competing candidate. To rationalize the stability of the above-mentioned structures in freestanding monolayer MoS_2, in this paper, we use finite-temperature first-principles techniques to tackle these questions. Based on the 0 K energetics of the four $1T$-like structures, dynamic characteristics of the $1T$ phase at high temperatures, potential-energy landscapes, and computed free energies, we show that the $1T'$ phase is the only succeeding low-symmetry structure from the $1T$ phase when temperature decreases, and the phase transition is of first order with significant order-disorder nature.

The remainder of this paper is organized as follows: A description of the computational method is provided in Sec. II. Section III reports and discusses the structural, energetic, and dynamical properties of the $1T$, $1T'$, $d1T$, and $1T''$ phases of monolayer MoS_2, the structural changes by cooling of the $1T$-MoS_2 from high temperature, the strain effect, and the ground state of other MoX_2 ($X = $ Se,Te) monolayer. Finally, we summarize the study in Sec. IV.

II. COMPUTATIONAL DETAILS

The first-principles density-functional theory (DFT) calculations were performed using the Vienna *ab initio* simulation package (VASP) [21,22], employing the Perdew-Burke-Ernzerhof (PBE) functionals and projector augmented-wave (PAW) method [23–25]. The orbitals of $4p^6 4d^5 5s^1$, $3s^2 3p^4$, $4s^2 4p^4$, and $5s^2 5p^4$ were explicitly treated as valence electrons for Mo, S, Se, and Te, respectively. A cutoff energy of 500 eV for the plane-wave basis set was used in all calculations. For geometry optimization, Monkhorst-Pack k meshes of $24 \times 24 \times 1$, $12 \times 24 \times 1$, $14 \times 14 \times 1$, and $12 \times 12 \times 1$ were used for the unit cell of the $1T$ (three atoms), $1T'$ (six atoms), $d1T$ (nine atoms) and $1T''$ (twelve atoms) phases, respectively. The external and internal structural parameters were fully relaxed until the Hellmann-Feynman force on each atom was less than 0.001 eV/Å, and the convergence threshold for self-consistent-field iterations was set to 10^{-8} eV. A vacuum space of 15 Å in the vertical direction was adopted to avoid interactions between neighboring images.

Zero-K phonon dispersion curves were computed using the direct supercell approach implemented in the PHONOPY [26] code, with the following supercell sizes: $6 \times 6 \times 1$, $3 \times 6 \times 1$, $4 \times 3 \times 1$, and $3 \times 3 \times 1$ for the $1T$, $1T'$, $d1T$, and $1T''$ phases, respectively. Convergence of phonon dispersion with respect to the supercell size was tested for the $1T$ phase, and $6 \times 6 \times 1$ was found to be adequate. Calculations of the finite-temperature phonons were carried out using

the temperature-dependent effective potential (TDEP) method [27–29], by extracting effective interatomic force constants taking the anharmonicity into account for a given temperature based on Born-Oppenheimer molecular-dynamics (MD) simulations using the VASP code adopting canonical ensembles (NVT). The temperature was controlled by using a Nosé thermostat. The MD simulations ran for at least 6000 steps for the $1T'$, $d1T$, and $1T''$ phases, and 20 000 steps for the $1T$ phase, with a time step of 2 fs. Note that the $6 \times 6 \times 1$ supercell in terms of the three-atom $1T$ unit cell can accommodate the structural distortions of the $1T'$, $d1T$, and $1T''$ phases. The Helmholtz free energies were calculated accurately by including anharmonic contributions using TDEP [29].

III. RESULTS AND DISCUSSION

A. Stable phase of freestanding MoS₂

The monolayer structure of the high-symmetry $1T$ phase (space group $P\bar{3}m1$) is shown in Fig. 1(a), in which the Mo atoms are octahedrally coordinated with six nearest-neighbor S atoms, resulting in an ABC stacking along the c direction considering the Mo and S atoms. More details of the structure are listed in Table I. The lattice constants and interatomic distances extracted from our relaxed structure are in good agreement with previous calculations [15,17].

Figure 1(b) shows the computed phonon dispersion curves of monolayer $1T$-MoS_2 along the high-symmetry path of $\Gamma(0, 0, 0)$-M(1/2, 0, 0)-K(1/3, 1/3, 0)-$\Gamma(0, 0, 0)$. Being consistent with other work [7], while most phonon frequencies are positive, significant soft phonon (imaginary frequencies) occurs at K and M points, indicating that this structure is dynamically unstable at zero K. The eigen displacement associated with the M point is illustrated in Fig. 1(c), which is characterized mainly by antipolar displacements with large in-plane components from the Mo atoms, together with antipolar out-of-plane displacements of the S atoms. The antipolar motion following the M-point mode causes doubling of the unit cell along the a direction, and relaxation of the distorted structure results in the $1T'$ phase [Fig. 1(d), space group $P2_1/m$]. Similarly, the distortion pattern and structure of the $d1T$ phase (space group $P31m$) are shown in Figs. 1(e) and 1(f). Still taking the $1T$ phase as reference, Mo atoms in the $d1T$ phase have in-plane trimerization, while the displacements of the S atoms involve both in-plane trimerization and out-of-plane displacements, giving rise to a $\sqrt{3} \times \sqrt{3}$ unit cell. The $1T''$ phase (space group $P3m1$) is associated with the soft phonon at M' $(1/2, 1/2, 0)$ point, which shares the same imaginary frequency as that of the M point. But the atomic distortions are different from $1T'$, yielding a 2×2 unit cell, and the resulting structure is shown in Figs. 1(g) and 1(h). Relative to $1T$, the Mo atoms in the $1T''$ phase trimerize around the S atoms, causing small out-of-plane displacements.

The structural parameters of the $1T'$, $d1T$, and $1T''$ phases are also listed in Table I. Compared with the $1T$ structure, the $1T'$ lattice constant b is almost unchanged (shrank by merely 0.1%), while a enlarges by 2.7% in the pseudo-$1T$ convention. On the other hand, both the $d1T$ and $1T''$ phases remain hexagonal and the pseudo-$1T$ lattice constants are larger by 1.8% and 1.2%, respectively. The interatomic distances also
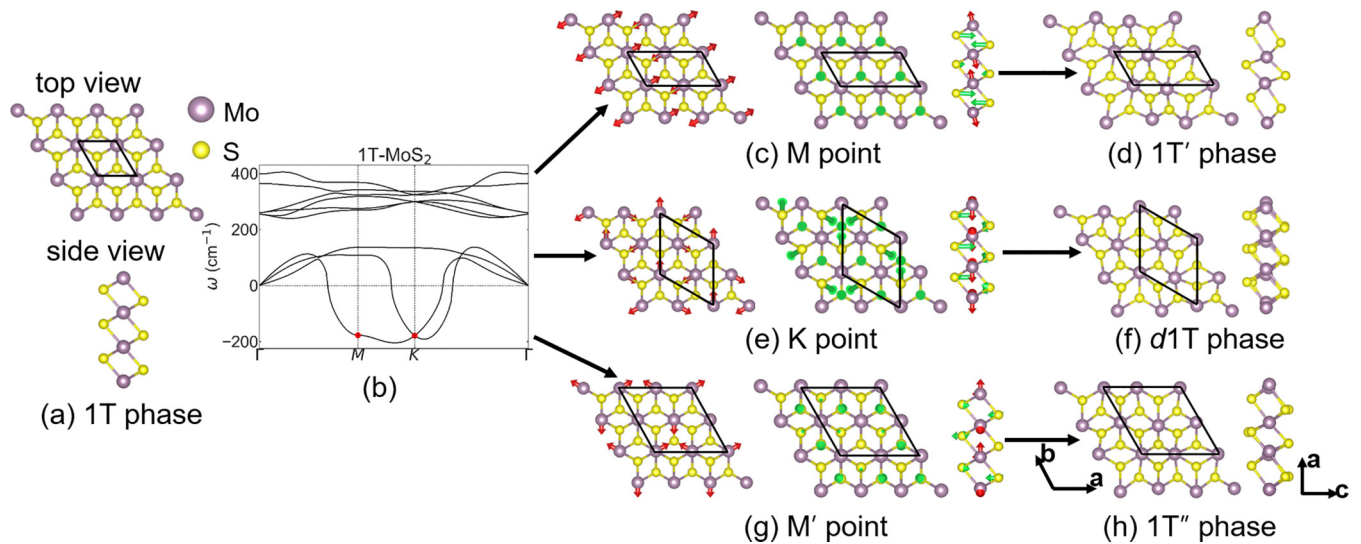
FIG. 1. Structures of the high-symmetry and distorted phases of monolayer MoS$_2$. (a) Top and side views of the 1T phase. (b) DFT calculated 0-K phonon spectrum of the 1T phase. (c), (d) The atomic displacement patterns of the Mo and S atoms, and the relaxed structure of the 1T' phase, originating from the soft mode at the M point. (e), (f) Same as the d1T phase, originating from the soft mode at the K point. (g), (h) Same as the 1T'' phase. The red and green arrows indicate the displacements of the Mo and S atoms relative to the 1T structure. The respective unit cells are illustrated with black lines.

reflect the structural differences. For instance, the distance between nearest-neighbor Mo-Mo ($d_{\text{Mo-Mo}}$) in the 1T phase is single valued at 3.185 Å, while in 1T' and 1T'' it splits into three lengths, and in d1T it splits into two lengths. The intermediate $d_{\text{Mo-Mo}}$ in 1T' and 1T'' is close to that of the 1T phase and is omitted in a previous report [17]. The shorter $d_{\text{Mo-Mo}}$ is distinctively different between 1T' (or 1T'') and d1T, i.e., 2.77 vs 3.02 Å, which can be used to characterize their differences.

As expected from the soft phonon modes, the calculated energies of the 1T', d1T, and 1T'' phases are all lower than that of the 1T phase, with relative energies of $\Delta E_{1T'} = -289.7$ meV/f.u., $\Delta E_{d1T} = -286.7$ meV/f.u. and $\Delta E_{1T''} = -206.4$ meV/f.u., respectively. The energy of the 1T'' phase is about 80.0 meV/f.u. higher than that of 1T' and d1T, which is consistent with the reported value in Ref. [17]. Given the much higher energy, the 1T'' phase is unlikely to be a stable polymorph of freestanding monolayer MoS$_2$. On the other hand, $E_{1T'}$ and E_{d1T} are very close, and both structures can be dynamically stable at zero K, as indicated by the absence of soft phonon in their dispersion curves [Figs. 2(a) and 2(b)]. Hence no further structural transition is implied from phonon instabilities, and the slightly lower

energy of the 1T' phase suggests that it is likely to be the ground state at low temperature. Note that strong soft phonon branches occur in the 1T'' phase at 0 K [see Fig. 2(c)], and its structure cannot remain stable during the MD runs at finite temperature between 100 and 800 K, so it will not be further considered.

The quantitative characterization of the structural distortions of the 1T' and d1T phases can be obtained using the crystallographic tool AMPLIMODE [30,31], as shown in Table II. The distortion of the 1T' phase is entirely due to the projected amplitude of the M$_2^-$ mode, while for the d1T structure, the main contribution is from the K$_3$ mode, with moderate and very small magnitudes from Γ$_1^+$ and Γ$_2^-$, respectively. The Γ$_2^-$ mode gives rise to an out-of-plane spontaneous polarization of the d1T phase, as also reported by Ref. [15].

Next, let us examine the occurring structure of monolayer MoS$_2$ at finite temperatures. Starting from the high-symmetry 1T phase, we first calculate the phonon dispersion at 1200 K using the TDEP method based on *ab initio* MD simulations. As shown in Fig. 3(a) (red curves), all frequencies are positive, implying that the 1T phase is stable at this temperature. Between 750 and 1200 K, the average structure remains 1T, and the dispersion curves changes slightly with temperature

TABLE I. DFT calculated lattice constants, nearest-neighbor interatomic distances, and energies of monolayer 1T-, 1T'-, d1T-, and 1T''-MoS$_2$, in comparison with previous first-principles computations.

	1T		1T'		d1T		1T''	
	This work	Ref. [17]	This work	Ref. [17]	This work	Ref. [15]	This work	Ref. [17]
a (Å)	3.185	3.17	6.543	6.55	5.615	5.62	6.446	6.44
b (Å)	3.185	3.17	3.182	3.18	5.615	5.62	6.446	6.44
$d_{\text{Mo-Mo}}$ (Å)	3.185	3.17	2.77, 3.18, 3.80	2.77, 3.18	3.02, 3.75	3.02	2.77, 3.23, 3.67	2.77, 3.26
E (eV/f.u.)[a]	0	0	−0.2897	−0.27	−0.2867	−0.288	−0.2064	−0.19

[a]The relative energy E is given using 1T-MoS$_2$ as the reference.
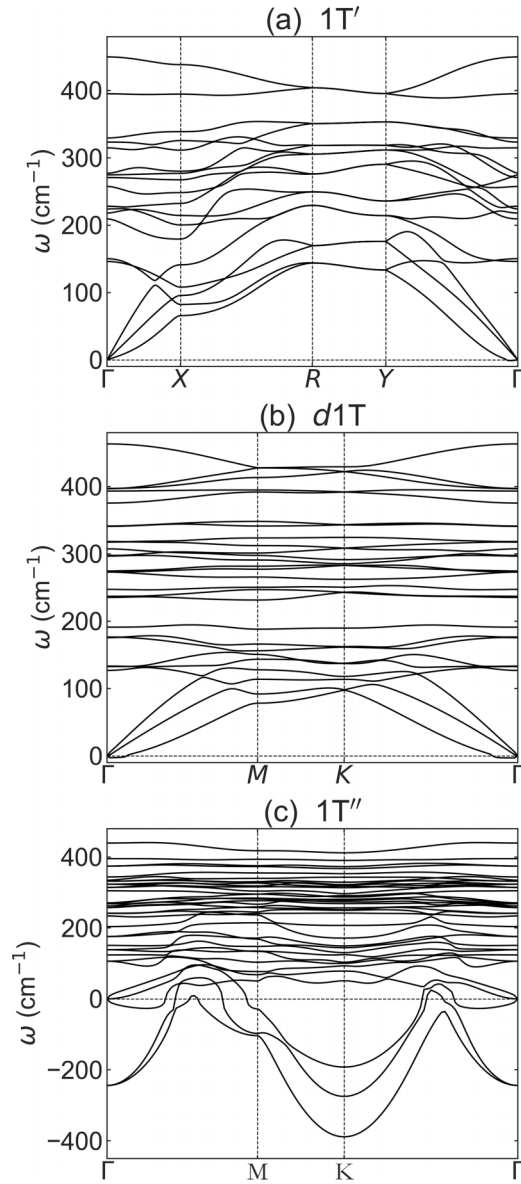
(a) 1T′

(b) d1T

(c) 1T″

FIG. 2. DFT calculated 0-K phonon dispersion curves of the (a) 1T′, (b) d1T, and (c) 1T″ phases.

[Fig. 3(a)]. Below 750 K, we numerically find that the average structure starts to deviate from the 1T phase, at least for a time span up to 40 ps in the MD simulations, which implies that a phase transition is likely to occur near 750 K. Temperature

TABLE II. Projected amplitudes of the 1T′ and d1T-MoS$_2$ monolayer structures in terms of the phonon modes of the high-symmetry 1T phase, using the crystallographic tool AMPLIMODE [30,31].

	1T′		d1T
Mode	Amplitude	Mode	Amplitude
M_2^-	0.2617	K_3	0.5233
Γ_3^+	0.0000	Γ_2^-	0.0467
Γ_1^+	0.0000	Γ_1^+	0.2640

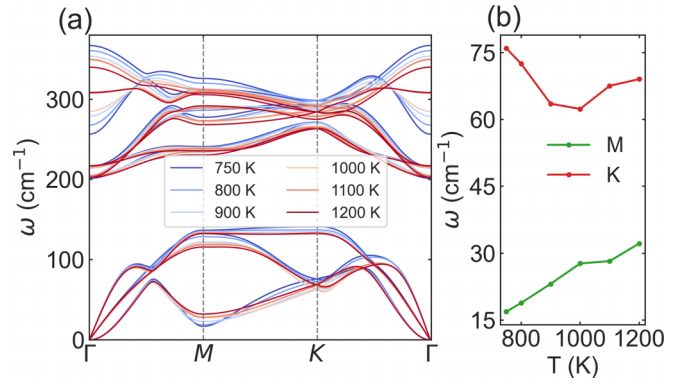FIG. 3. Calculated finite-temperature phonons of the 1T phase. (a) Phonon dispersion curves at various temperatures from 750 to 1200 K. (b) Frequencies of the phonons at M and K points as a function of temperature.

dependencies of the phonon frequencies at M and K points are shown in Fig. 3(b). Interestingly, the K-point mode does not soften with respect to the decrease of temperature, whereas the M-point frequency decreases rather linearly from 32.18 cm^{-1} at 1200 K to 16.89 cm^{-1} at 750 K. The lower and softening frequency from the M-point mode, rather than the K point, suggests that the 1T phase may transform into the 1T′ phase below 750 K. Nevertheless, since the M-point mode does not become fully soft (i.e., zero frequency) near the transition point, it is likely to be a first-order transition, instead of second order.

The nature of the first-order transition, as well as the dynamical feature of the 1T at high temperature, can be further elucidated from the correlation functions of the atom pairs, which is related to the probability of finding one atom from another atom at a given distance. Figure 4(a) reports the
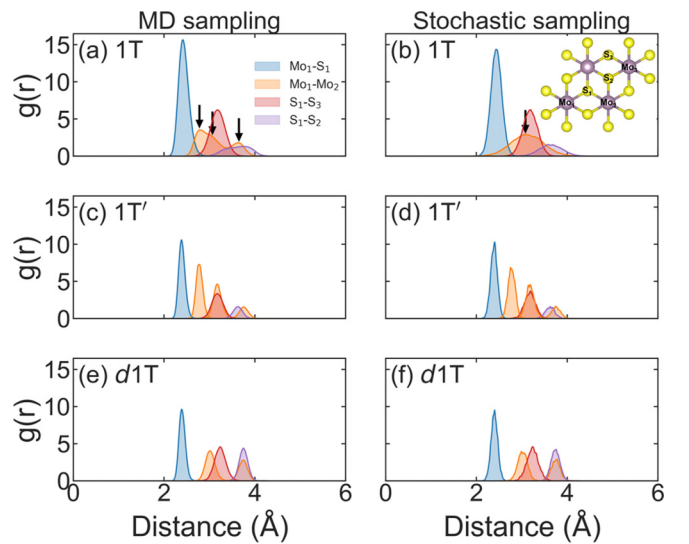

FIG. 4. Comparison of the calculated pair correlation functions according to (a), (c), (e) *ab initio* MD sampling for the 1T (at 800 K), 1T′ (at 500 K), and d1T phases (at 500 K), respectively, and (b), (d), (f) stochastic sampling for the same phases. Black arrows point to the differences in the 1T phase.
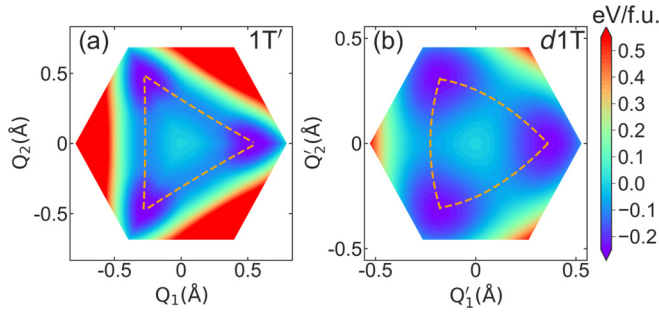
FIG. 5. Potential-energy landscape of monolayer MoS$_2$. (a) DFT calculated 0-K PES as functions of two-dimensional reaction coordinates Q_1 and Q_2, with the minima corresponding to the 1T′ phase. (b) PES as functions of two-dimensional reaction coordinates Q_1' and Q_2', with the minima corresponding to the d1T phase. The minimum-energy paths among the minima are denoted by dashed lines.
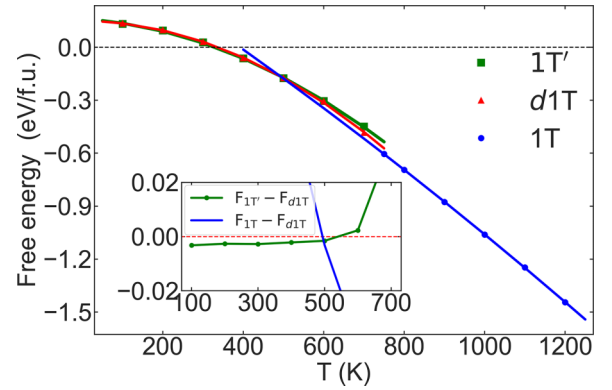

FIG. 6. Calculated Helmholtz potential-energy surfaces of the $1T, 1T', d1T$ phases as a function of temperature. The solid symbols denote calculated data using TDEP, and the solid lines are curves from quadratic fitting. The inset highlights the free-energy difference, relative to that of the $d1T$ phase.

calculated pair correlation function $g(r)$ at 800 K based on the MD simulation. For comparison, we also plot $g(r)$ from stochastic sampling [Fig. 4(b)], where harmonic oscillation of the phonons of the 1T phase is assumed at the same temperature of 800 K, which yields Gaussian distribution for each pair. The main noticeable difference between the two sampling schemes lies in the Mo$_1$-Mo$_2$ pair, which has a single peak with stochastic sampling but splits into three distances for MD sampling. Similar behavior is found for all studied temperatures from 750 to 1200 K, except that with increasing temperature the distance between the splitting peaks decreases, and the intermediate peak near 3.2 Å shrinks. It means that the 1T phase at high temperature is not simply a harmonic 1T structure but an average structure as a result of dynamic hopping of other structures, which is associated with the characteristic of an order-disorder type transition when symmetry lowering of the average structure occurs at a lower temperature.

For comparison, we also plot the pair correlation functions of the 1T′ [Figs. 4(c) and 4(d)] and d1T [Figs. 4(e) and 4(f)] phases, based on MD simulations at 500 K, at which both phases can be stable (or metastable). The MD and stochastic samplings yield almost identical $g(r)$ for these two structures, which means they are indeed their respective harmonically stimulated structures at finite temperatures. And the splitting peaks of Mo$_1$-Mo$_2$ match very well to the $d_{\text{Mo-Mo}}$ lengths of the zero-K 1T′ and d1T structures [Figs. 4(c) and 4(e) and Table I]. More interestingly, the Mo$_1$-Mo$_2$ peak positions of the 1T phase [Fig. 4(a)] resemble those of the 1T′ phase, in particular the three peak positions at 2.8, 3.1, and 3.8 Å, whereas the lower peak position and missing intermediate peak from the d1T phase is inconsistent.

To better illustrate the order-disorder nature of the transition and the hopping mechanism, we calculate the potential-energy surfaces (PESs) considering two scenarios: (i) hopping among equivalent 1T′ minima, and (ii) hopping among equivalent d1T minima. Two-dimensional contour plots of the PES with respect to the distortions of the 1T′ and d1T phases with the 1T structure as reference are shown in Figs. 5(a) and 5(b). Here Q_1 and Q_2 (or Q_1' and Q_2') are compositive transition coordinates determined by the two-dimensional in-

plane displacement vectors with the 1T structure as origin. For 1T′, there are three equivalent energy minima formed by 120° rotation of the displacement patterns [see Fig. 1(c)], while for d1T, only three degenerate minima of positive polarization are shown and one can imagine the other three with negative polarization and the same energy [see Fig. 1(e)]. Dynamic hopping among the equivalent minima with equal chance can result in the 1T structure, i.e., $Q_1 = Q_2 = 0$ or $Q_1' = Q_2' = 0$ in the PES. Furthermore, the 1T energy is 289.7 and 286.7 meV/f.u. higher than that of the 1T′ and d1T phases, respectively; however, the three minima are connected by alternative low-energy barrier pathways [dashed lines in Figs. 5(a) and 5(b)] without passing through the high-symmetry 1T point. Therefore, the high-temperature 1T phase is likely to be an average structure formed by jumping among the energy-degenerate distorted structures, which can also explain the splitting of the Mo$_1$-Mo$_2$ distance in the calculated pair correlation function [Fig. 4(a)]. It is also interesting to point out that the 1T′ phase not only has a slightly lower energy, but the associated energy barrier is also slightly lower than that of the d1T case, i.e., 173.1 vs 178.0 meV/f.u.

To find the most stable structure when the 1T phase becomes unstable with decreasing temperature, we calculate the Helmholtz free energies as a function of temperature for the 1T, 1T′, and d1T phases (Fig. 6), at temperatures that they can be stabilized, i.e., above 750 K for 1T, and below 600 K for 1T′ and d1T. Between 600 and 750 K, the average structure is neither 1T′ or d1T nor 1T within an affordable time span of MD simulations. To obtain the transition point, quadratic fitting is used to extend data to the intermediate-temperature region. As expected, the 1T phase has the lowest free energy at high temperature, while the 1T′ and d1T phases are competing at low temperatures. For better resolution, we plot the difference of free energies relative to the d1T phase in the inset of Fig. 6. Interestingly, the three curves cross almost at the same point corresponding to the temperature of 500 K, below which only the 1T′ phase is stable. It is worth noting that, albeit the small free-energy difference between 1T′ and d1T, the difference is robust from 500 to 100 K and is persistently increasing, e.g., 3.2 meV/f.u. at 100 K, which
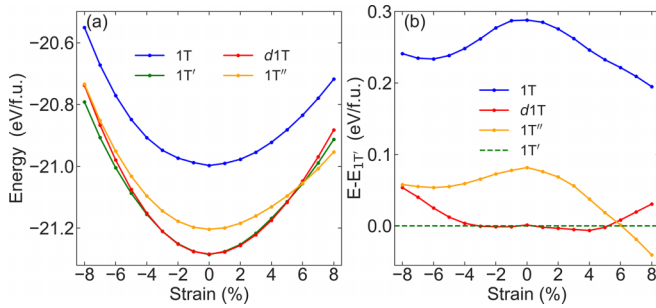
FIG. 7. (a) DFT calculated total energy as a function of strain for various phases of MoS_2. (b) Total energy as a function of strain for various phases of MoS_2, with the $1T'$ phase as reference (set to zero).

is very close to the 0-K energy difference of 3.0 meV/f.u. (Table I).

Therefore, the previously predicted ferroelectric $d1T$ phase is unlikely to be stable compared with the $1T'$ phase from low to high temperatures. Although the difference in energy or free energy is rather small, e.g., about 3.0 meV/f.u., statistically it can forbid the occurrence of $d1T$ at a large scale. Although $d1T$ and $1T''$ do not appear to be stable in freestanding monolayer MoS_2, they may be stabilized via strain or extrinsic means, such as introduction of defects, substitution, substrate, or solvent environment, etc. In fact, this may explain the observed $1T''$ phase in lithiated MoS_2 flakes [20]. Moreover, it is worth to mention that the energy barrier between $1T'$ or $d1T$ minima (178.0 meV/f.u., see Fig. 5) is significantly lower than the barrier between the 2H and $1T'$ phases (640.0 meV/f.u.) [32,33], allowing the $1T$-like phase to be metastable at even elevated temperatures.

B. Strain effect on the structural stability of MoS_2

Although the $1T'$ phase is predicted to be stable at low temperature in freestanding MoS_2 monolayer, the situation may change under strained conditions. By applying biaxial strain ranging from -8% to $+8\%$, the computed 0-K total energies of the $1T$, $1T'$, $d1T$, and $1T''$ structures are plotted in Fig. 7. While the $1T$ phase remains high in energy, the $1T'$ and $d1T$ phases compete in the vicinity of zero strain, with the $1T'$ phase being most stable at zero strain and the $d1T$ phase being slightly lower in energy than $1T'$ for both compressive and tensile strains in the range of -3% to -1% and 1% to 5%, respectively. And interestingly, the $1T''$ phase has the lowest energy if the tensile strain is larger than 6%.

We further select -2% and $+2\%$ strain and calculate the pair correlation functions based on MD simulations at 800 K, at which the average structure is the high-symmetry $1T$ phase, as shown in Fig. 8. With -2% strain, although the $d1T$ phase has slightly lower energy than that of $1T'$, the pair correlation function show signature of the bond lengths of the $1T'$ phase, indicating that the $1T'$ phase is likely to be more stable at elevated temperatures. On the other hand, with $+2\%$ strain, the pair correlation function only has two peaks for the Mo-Mo distances, which match the bond lengths of the $d1T$ phase. This is also consistent with the fact that the energy difference between $d1T$ and $1T'$ is more substantial under tensile strain [Fig. 7(b)].
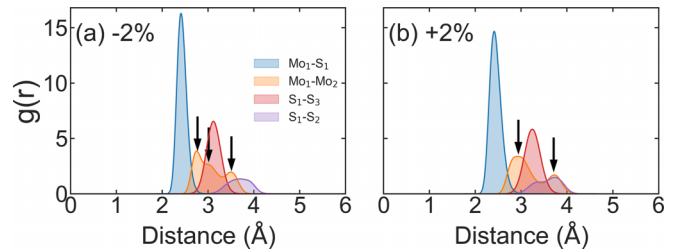

FIG. 8. Pair correlation functions of $1T$-MoS_2 under (a) -2% and (b) 2% strains at 800 K.

C. Stable phases of freestanding MoX_2 ($X = Se$, Te)

$1T'$ phase is also found to be the ground state of other freestanding MoX_2 monolayer, with X being Se or Te. As shown in Fig. 9(a), the total energy of the $1T'$ phase is slightly lower than $d1T$ for MoS_2, and its energy decreases more than the $1T''$ and $d1T$ phases as the anion changes from S to Te, for instance, its relative energy with respect to the $d1T$ (or $1T''$) phase increases from 3.0 to 185.8 meV/f.u. (or 83.3 to 183.7 meV/f.u.). In other words, the $1T'$ phase becomes increasingly stable as the chalcogen atom gets larger. Interestingly, the soft mode at the M point are more significant than that at the K point in $MoSe_2$ and $MoTe_2$ [Fig. 9(b)], suggesting that the $1T'$ phase derived from soft modes at the M point is likely to be more stable than the $d1T$ phase derived from soft modes at the K point.
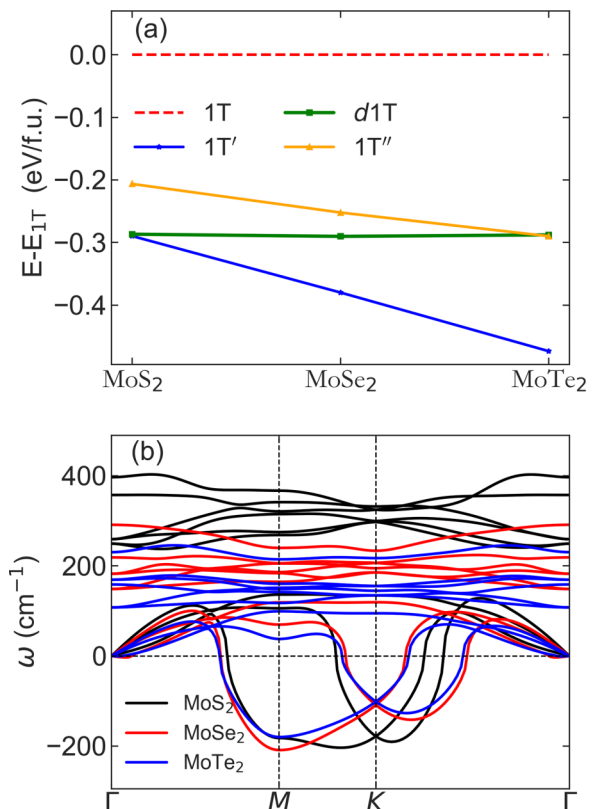

FIG. 9. (a) Total energy for various phases of MoX_2, with the $1T$ phase as reference (set to zero). (b) DFT-calculated 0-K phonon spectrum of the $1T - MoX_2$.
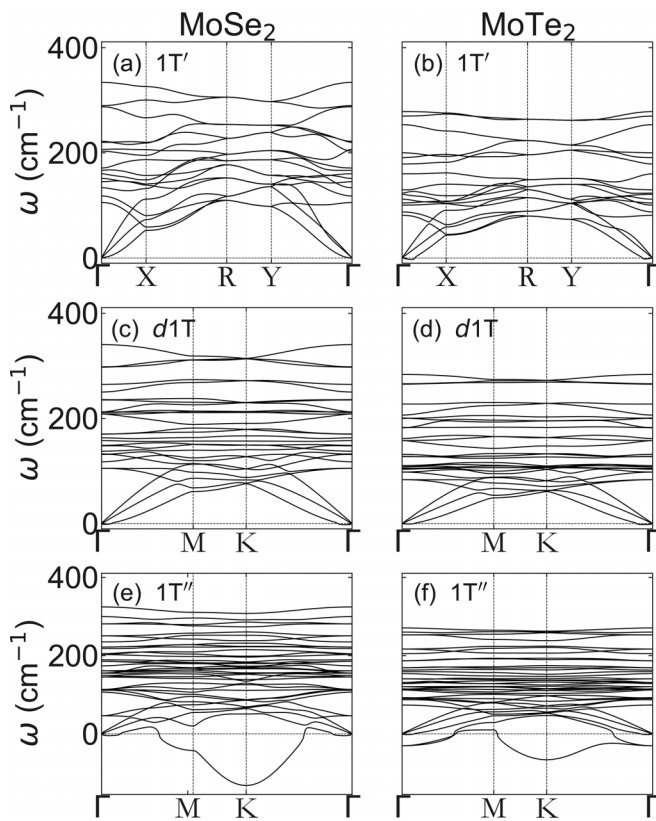
FIG. 10. DFT calculated 0-K phonon dispersion curves of the 1*T′*-, *d*1T- and 1*T″*-MoX_2.

Dynamical stability of the 1*T′* phase of MoSe$_2$ and MoTe$_2$ is confirmed by the 0-K phonon spectra (Fig. 10). The *d*1T phase is also dynamically stable, but in contrast, the 1*T″* phase has strong soft phonon branches in all three compounds [Figs. 2(c), 10(e), and 10(f)]. This further indicates that for MoX_2, the 1*T″* phase is unlikely to be the stable structure at low temperature. A hint of the stable phase derived from the 1*T* phase upon cooling can be seen from the pair correlation functions, obtained based on the MD simulations at 800 K. As depicted in Fig. 11, the number and positions of peaks corresponding to the Mo-Mo pairs match that of the 1*T′* phase for these three MoX_2. This is consistent with the 0-K ground state according to the total energies, suggesting that the 1*T′* phase is likely to be the stable phase for freestanding monolayer MoS$_2$, MoSe$_2$, and MoTe$_2$ at both low and finite temperatures.

IV. CONCLUSIONS

In summary, we have combined density-functional theory calculations and temperature-dependence effective potential
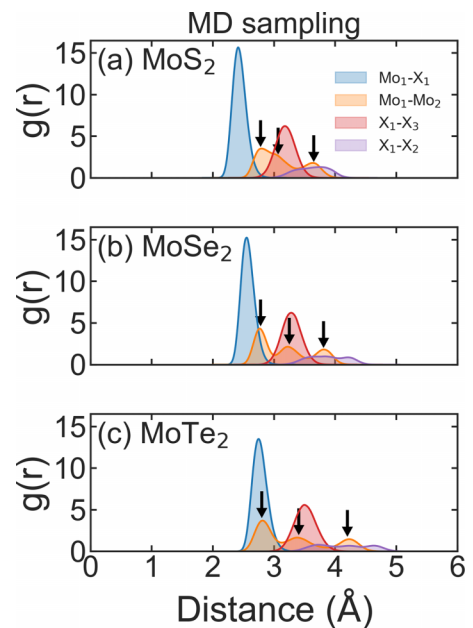

FIG. 11. The pair correlation functions were calculated and compared based on *ab initio* MD sampling for MoS$_2$, MoSe$_2$, and MoTe$_2$ at 800 K, denoted as (a), (b), and (c), respectively.

method to investigate the stable structures of freestanding monolayer MoS$_2$ when cooling from high temperature in the 1*T* phase. By considering three candidate low-temperature phases derived from the soft phonons at M, K, and M′ points, viz., the 1*T′*, *d*1T, and 1*T″* phases, respectively, the nonpolar 1*T′* phase is found to be the most stable one from zero temperature up to the transition point to the 1*T* phase. On the other hand, the two ferroelectric hexagonal phases, i.e., *d*1T and 1*T″*, are unlikely to be stable due to higher free energy or total energy. We also show that the 1*T*-to-1*T′* transition should be of the order-disorder type, originated from hopping among local energy minima of the 1*T′* structures. Freestanding MoSe$_2$ and MoTe$_2$ are likely to share the same ground state, while strain engineering is found to be an effective means to render other stable structures.

[1] J. Tan, S. Li, B. Liu, and H. Cheng, Small Struct. **2**, 2000093 (2021).

[2] X. Li, L. Tao, Z. Chen, H. Fang, X. Li, X. Wang, J. Xu, and H. Zhu, Appl. Phys. Rev. **4**, 021306 (2017).

[3] K. S. Novoselov, A. Mishchenko, A. Carvalho, and A. H. Castro Neto, Science **353**, aac9439 (2016).

[4] S. Haastrup, M. Strange, M. Pandey, T. Deilmann, P. S. Schmidt, N. F. Hinsche, M. N. Gjerding, D. Torelli, P. M.

Larsen, A. C. Riis-Jensen *et al.*, 2D Mater. **5**, 042002 (2018).

[5] Z. Sun, T. Ma, H. Tao, Q. Fan, and B. Han, Chem **3**, 560 (2017).

[6] S. Z. Butler, S. M. Hollen, L. Cao, Y. Cui, J. A. Gupta, H. R. Gutiérrez, T. F. Heinz, S. S. Hong, J. Huang, A. F. Ismach, E. Johnston-Ha, M. Kuno, V. V. Plashnitsa, R. D. Robinson, R. S. Ruoff, S. Salahuddin, J. Shan, L. Shi, M. G. Spencer, M. Terrones *et al.*, ACS Nano **7**, 2898 (2013).

[7] S. N. Shirodkar and U. V. Waghmare, Phys. Rev. Lett. **112**, 157601 (2014).

[8] B. Radisavljevic, A. Radenovic, J. Brivio, V. Giacometti, and A. Kis, Nat. Nanotechnol. **6**, 147 (2011).

[9] R. Kappera, D. Voiry, S. E. Yalcin, B. Branch, G. Gupta, A. D. Mohite, and M. Chhowalla, Nat. Mater. **13**, 1128 (2014).

[10] M. A. Py and R. R. Haering, Can. J. Phys. **61**, 76 (1983).

[11] R. Kappera, D. Voiry, S. E. Yalcin, W. Jen, M. Acerce, S. Torrel, B. Branch, S. Lei, W. Chen, S. Najmaei, J. Lou, P. M. Ajayan, G. Gupta, A. D. Mohite, and M. Chhowalla, APL Mater. **2**, 092516 (2014).

[12] Y. C. Lin, D. O. Dumcenco, Y. S. Huang, and K. Suenaga, Nat. Nanotechnol. **9**, 391 (2014).

[13] M. Acerce, D. Voiry, and M. Chhowalla, Nat. Nanotechnol. **10**, 313 (2015).

[14] A. Singh, S. N. Shirodkar, and U. V. Waghmare, 2D Mater. **2**, 035013 (2015).

[15] J. H. Choi and S. H. Jhi, J. Phys.: Condens. Matter **32**, 045702 (2020).

[16] D. Voiry, A. Mohite, and M. Chhowalla, Chem. Soc. Rev. **44**, 2702 (2015).

[17] S. S. Chou, N. Sai, P. Lu, E. N. Coker, S. Liu, K. Artyushkova, T. S. Luk, B. Kaehr, and C. J. Brinker, Nat. Commun. **6**, 8311 (2015).

[18] Y. Yu, G. H. Nam, Q. He, X. Wu, K. Zhang, Z. Yang, J. Chen, Q. Ma, M. Zhao, Z. Liu, F. Ran, X. Wang, H. Li, X. Huang, B. Li, Q. Xiong, Q. Zhang, Z. Liu, L. Gu, Y. Du *et al.*, Nat. Chem. **10**, 638 (2018).

[19] X. R. Qin, D. Yang, R. F. Frindt, and J. C. Irwin, Ultramicroscopy **42–44**, 630 (1992).

[20] A. Lipatov, P. Chaudhary, Z. Guan, H. Lu, G. Li, O. Crégut, K. D. Dorkenoo, R. Proksch, S. Cherifi-Hertel, D. F. Shao, E. Y. Tsymbal, J. Íñiguez, A. Sinitskii, and A. Gruverman, npj 2D Mater. Appl. **6**, 18 (2022).

[21] G. Kresse and J. Furthmüller, Phys. Rev. B **54**, 11169 (1996).

[22] G. Kresse and D. Joubert, Phys. Rev. B **59**, 1758 (1999).

[23] P. Hohenberg and W. Kohn, Phys. Rev. **136**, B864 (1964).

[24] P. E. Blöchl, Phys. Rev. B **50**, 17953 (1994).

[25] J. P. Perdew, K. Burke, and M. Ernzerhof, Phys. Rev. Lett. **77**, 3865 (1996).

[26] A. Togo and I. Tanaka, Scr. Mater. **108**, 1 (2015).

[27] O. Hellman, I. A. Abrikosov, and S. I. Simak, Phys. Rev. B **84**, 180301(R) (2011).

[28] O. Hellman and I. A. Abrikosov, Phys. Rev. B **88**, 144301 (2013).

[29] O. Hellman, P. Steneteg, I. A. Abrikosov, and S. I. Simak, Phys. Rev. B **87**, 104111 (2013).

[30] D. Orobengoa, C. Capillas, M. I. Aroyo, and J. M. Perez-Mato, J. Appl. Crystallogr. **42**, 820 (2009).

[31] J. M. Perez-Mato, D. Orobengoa, and M. I. Aroyo, Acta Crystallogr., Sect. A: Found. Crystallogr. **66**, 558 (2010).

[32] Y. Linghu, N. Li, Y. Du, and C. Wu, Phys. Chem. Chem. Phys. **21**, 9391 (2019).

[33] H. H. Huang, X. Fan, D. J. Singh, and W. T. Zheng, Phys. Chem. Chem. Phys. **20**, 26986 (2018).